NATIONAL AERONAUTICS AND SPACE ADMINISTRATION

Technical Memorandum 33-710

Numerical Orbit Integration Efficiency of the Delaunay-Similar Elements

Sam Pierce

JET PROPULSION LABORATORY
CALIFORNIA INSTITUTE OF TECHNOLOGY
PASADENA, CALIFORNIA

October 15, 1974

NATIONAL AERONAUTICS AND SPACE ADMINISTRATION

Technical Memorandum 33-710

Numerical Orbit Integration Efficiency of the Delaunay-Similar Elements

Sam Pierce

JET PROPULSION LABORATORY
CALIFORNIA INSTITUTE OF TECHNOLOGY
PASADENA, CALIFORNIA

October 15, 1974

PREFACE

The work described in this report was performed by the Mission Analysis Division of the Jet Propulsion Laboratory.

ACKNOWLEDGEMENTS

The author gratefully acknowledges NASA Goddard Space Flight Center for supporting this study under research Grant NGR-05-071-005; the Jet Propulsion Laboratory for producing this publication; Dr. C. E. Velez and Mr. A. J. Fuchs for pertinent advice and information; and my students Mr. Ernest J. Spiehler and Mr. J. R. Ruzicska for their programming assistance.

CONTENTS

ABSTRACT

Orbit equations with a set of conservative and a set of non-conservative perturbing potentials are considered. Scheifele's DS formulation of these equations has dependent variables similar to Delaunay's orbital elements with the true anomaly as the independent variable. Efficiency curves of computing cost v.s. accuracy are constructed for Adams integrators of orders 2 through 15 with several correcting algorithms and for a Runga-Kutta integrator. Considering stability regions, choices are made for the optimally efficient integration modes for the DS elements. Integrating in these modes reduces computing costs for a specified accuracy.

1.0 INTRODUCTION, CONCLUSIONS

1.1 Introduction, Summary

This report is one study which is part of a larger NASA effort by many researchers to increase the accuracy and decrease the computing costs of generating orbits. The results will improve efficiency of mission design, operations, scientific applications and other processes where orbit generation is an integral part.

By a "correcting algorithm" is meant a particular predict-correct process such as PECE which is a prediction followed by a function (differential equation) evaluation, a correction, and another evaluation.

An "integration mode" consists of an algorithm (or variable algorithm method) and an order (or variable order) method.

An " orbit generator" consists of the formulation of the equations of motion (Cowell, VOP, DS, ...), an integrator, and an integration mode.

An "efficiency curve" is a plot of error v.s. cost for one problem and one orbit generator.

Since the cost of a particular stepsize depends on the algorithm, the cost of function evaluations on the formulation, and the cost of CPU time on the computer installation, there is no universally acceptable cost scale. All three scales are given in our figures.

Imagine placing a set of efficiency curves, each with a different

algorithm (e.g. Figures 9 - 12 for J_2), in order of increasing influence of the corrector to form a three dimensional graph of h v.s. error v.s. algorithm. Each figure is a cross section of constant "algorithm".

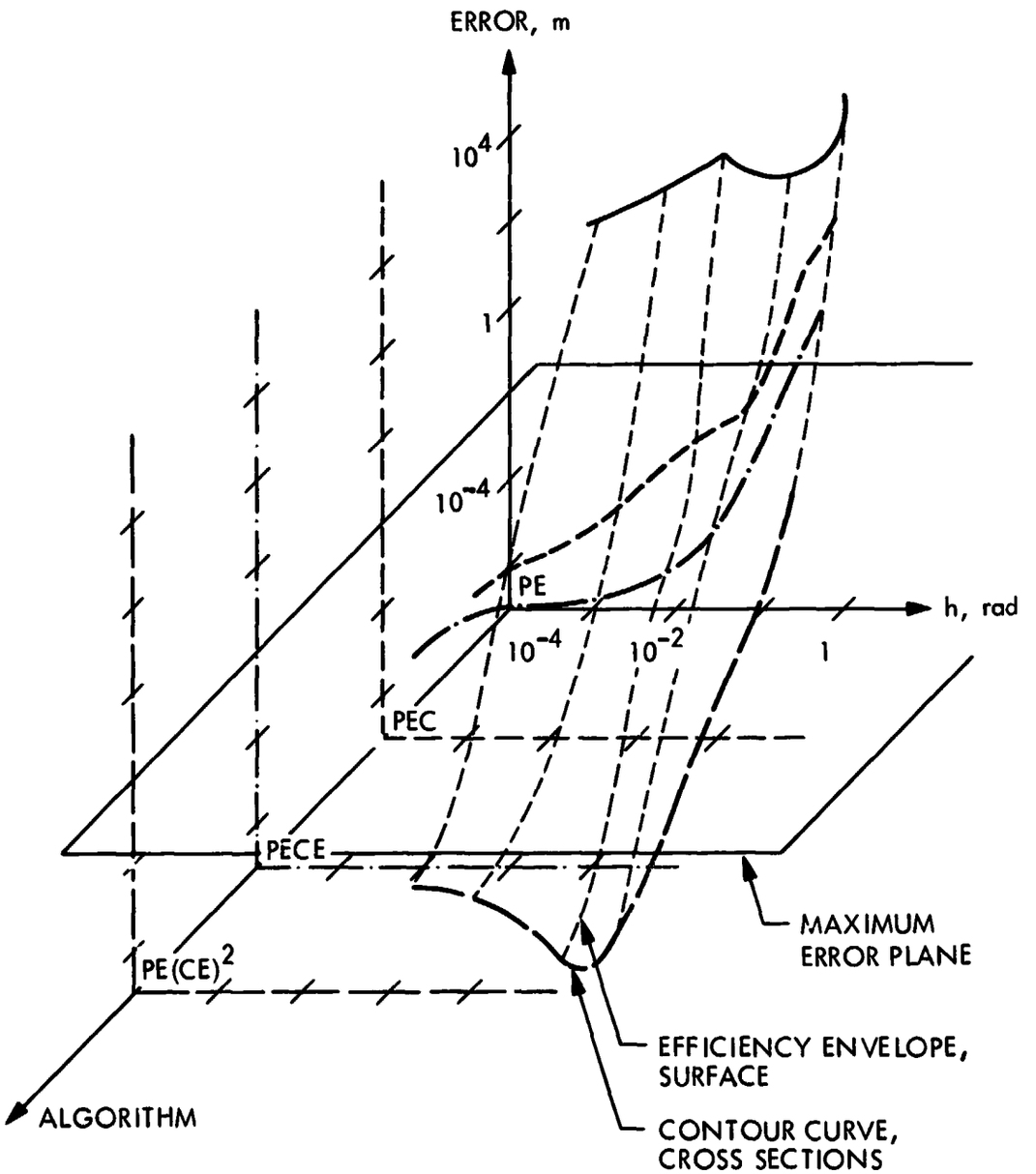

Definition: The "efficiency envelope" is the surface constructed by choosing the low points in the above schematic by choosing that order giving the smallest error for each algorithm and step-size.

Choosing the low points in each cross section, we get a contour curve of the efficiency envelope. This process optimizes over the variable "order" leaving the other parameters of algorithm, integrator, and formulation. Superimposing the contour curves, as in Figure 16, we project the efficiency envelope onto the h-error plane. Figure 17 does the same for the J_2 and lunar perturbations.

We interpret optimizing over the parameter "algorithm" as specifying an h-algorithm plane perpendicular to the error axis (at 10^{-2} m in the schematic) and searching the lower-right (large h) side of the intersection of this plane with the efficiency envelope. We thus choose the algorithm and order which allows the largest h and the smallest computing time, subject to the error criteria. The variable correcting and partial correcting algorithms (such as used in GSFC program GTDS) essentially refine the grid in the algorithm dimension thus allowing a choice of a more optimal integration mode.

This report accomplishes this optimization for the DS formulation [15] and Adams fixed step integrators. A range of a factor of 10^3 in h gives a complete idea of stability and accuracy that is possible. In one study [11] the Cowell formulation is optimized over several fixed step integrators. Another study [1] shows the DS formulation compares favorably to others. Two relatively new integrators that should be further studied due to their increased accuracy and stability are the back-correcting [2]

and the cyclic [5, 21] in particular the optimized cyclic [14].

The overall effort is to search for the most efficient orbit generator by considering the parameters "formulation" and "integrator," thus adding two dimensions to the geometry for a total of 5. Analytical studies such as [12] and [17] will help fill in the now four dimensional efficiency envelope surface by considering relationships between formulation and integrator. So will numerical studies that consider different formulations such as [1], [4], [9], [13], [19], [20].

Statement of the Overall Effort:

Minimize cost as a function of formulation, integrator, integration mode, error

Subject to the Constraint: error $\leq$ k.

The approach presently taken for this enormous, nonlinear, constrained optimization problem is essentially a numerical mapping routine, i.e., choose an orbit, formulation, integrator, integration mode, stepsize, and then integrate to get a point on the surface. This approach is quite costly due to the many parameter combinations that must be studied. Using emperical experience and analytical studies will reduce the number of parameter combinations it is necessary to consider. We also recommend studying the feasibility of using a more efficient numerical optimization procedure [14] to find the overall most efficient orbit generator for each problem. Once done the savings in applying these generators will be considerable.

1.2 Conclusions

1. In the DS formulation α_1 (true anomaly) and α_4 (time element) are the only variables termed "fast" and α_4 is 10^5 faster than α_1. With J_2 the variation in α_5 and α_6 increases to the order of α_1.

   With J_2 and lunar perturbations α_5, α_6, and α_7 become 10^2 to 10^3 faster than α_1, their fastest variation is near apogee, Adams efficiency decreases by about 10^3 (R-K by 10^7) and stability problems enter. For stability, stepsize control is advisable in this vicinity, but this should be done carefully.

2. The dynamic and numerical stability of the OB formulation depends on that of the DS and on the second partials of the DS-OB generating function.

3. The order 7 R-K integrator has the slope of an order 10 method, while Adams generally act like they are lower order than they ideally are. Despite this, Adams fixed step is overall more efficient than R-K fixed or variable step. (At higher accuracies with lunar perturbations R-K variable step is slightly better.) For best efficiency, Adams variable step should probably be used near perturbations other than those due to the central body.

   The remaining conclusions are concerned with Adams integrators.

4. Numerically DS is very stable with J_2; order 15 is stable at only 7 steps per revolution. With the moon order 8 remains stable at this large h but higher orders have smaller stability regions. The stability

region becomes smaller with more corrections, also.

5. With J_2, higher orders and more correcting generally yield steeper curves; however, orders greater than 12 do not significantly improve efficiency. For small h all orders are parallel with slope 1.0 or 2.0 depending only on algorithm. With J_2 and moon at all h, the curves for different orders generally stick to a tight bundle with slope 1.5 to 2.5 depending only on algorithm. This behavior is not typical truncation or roundoff. The explanation is hypothesized to lie in the truncation error coupling of formulation to integrator.

6. With J_2, $PE(CE)^2$ order 12 or 15 is most efficient for errors $\leq$ 1 m. The most efficient for larger errors is PEC order 12 or 15. With J_2 and moon, $PE(CE)^2$ order 8 is most efficient and stable for errors $\leq$ 100 m. For larger errors PEC order 6 is best.

2.0 PROBLEM FORMULATION

2.1 Problem Sets

The greatest use of this formulation is likely to be on highly eccentric orbits. The orbits considered have initial conditions:

X(1) = .9000000000000000D 04	α(1) = -.1120590941151 22D 01
X(2) = -.1000000000000000D 04	α(2) = -.1742056137944 42D 01
X(3) = -.8000000000000000D 03	α(3) = .2765928190018 92D 01
X(4) = .2600000000000000D 05	α(4) = -.7285994650403 27D 05
X(5) = -.4123110000000000D 01	α(5) = .2418154059291 12D 06
X(6) = .8000000000000000D 01	α(6) = .7163419425915 42D 05
X(7) = -.2000000000000000D 01	α(7) = .6787689000000000D 05
X(8) = .1358707695979 75D 01	α(8) = .1358707695979 75D 01

$a = 1.5 \times 10^5$ km, e = .96, $i = 18^\circ 40'$, $p = .58 \times 10^6$ secs = 6.8 days,

where $X_{1, 2, 3}$ is the Cartesian position in km, $X_{5, 6, 7}$ is the Cartesian velocity in km/sec, X_4 is the physical time, X_8 is the total energy, $\alpha_{1, \ldots, 8}$ is the DS vector described later, and a, e, i, and p have the usual meanings.

We consider two sets of perturbations: (1) the full J_2, conservative, term of the Earth's potential $= -\frac{\epsilon}{r^3}\left(\frac{1}{3} - \left(\frac{X_3}{r}\right)^2\right)$ where $\epsilon = 2.627622224 \times 10^{10}$. (2) The above J_2 term plus the non-conservative (time varying) force due to the fictitious moon moving in a circular orbit at a distance 3.844×10^5 km from the Earth with an angular velocity 2.66×10^{-6} radians/sec (p = 27.4 days) and gravitational constant times mass = 4902.66. This fictitious moon will have the same effect on the integrators as the real moon and will avoid ephemeris difficulties in this testing phase of the work.

A sketch of the geometry during the first orbit is shown in Figure 1.

Figure 2 graphs the Earth-satellite distance, r, and the physical time, X_4, v.s. the true anomaly, T, for J_2 only. Figure 3 shows the same for J_2 and the moon. The final time specified on input is $t_f = 1.494 \times 10^6$ secs, just before three revolutions and just after apogee. With J_2 only $T_f = 16.895$ radians, $r = 2.756 \times 10^5$ km and with J_2 and the moon $T_f = 16.899$ radians, $r = 2.736 \times 10^5$ km.

2.2 Formulations

In integrating elliptical orbits much overhead and interpolation error can result from using a variable step algorithm to reduce local truncation errors near pericenter. One means of avoiding this is to use automatic time step regulation [10], [16]. Transform the independent variable from t to s by using

$$dt/ds = cr^n \quad . \tag{2.2-1}$$

Taking equal steps of size Δs will automatically yield smaller time steps, $\Delta t \sim cr^n \Delta s$, when r is small. Thus, the choice of n affects the efficiency of the integration [12].

An interesting analysis by Velez [17] shows the effect on the dynamic stability of the transformed equations of motion and, since this is coupled to the numerical stability of the integrator, the stability of the whole orbit generation process is also affected by the choice of n. He finds $n = 1.5$ best for the time regularized Cowell formulation with a fixed step Adams integrator. The choice is difficult since small n yield less dynamic stability and larger n yield less numerical stability.

Another problem with time regularization is that to get the position

at a final physical time the time equation (2.2-1) must be integrated giving timing errors. Multiplying this error by the velocity we get an implicit error in the position which must be added to the explicit position error. Several researchers, including Baumgarte, Stiefel [3], and Nacozy, have improved timing accuracy and stability by adding control terms or energy surface considerations to the equations of motion.

In integrating orbits that are basically two body, advantage can be taken of the two body analytic solution by transforming the dependent variables to the two body elements. These "variation of parameter" methods exactly solve the two body portion of the motion [16] and allow larger integration steps to be taken. Variable stepsize is still advisable since the elements change fastest near pericenter.

For this reason, authors have recently combined the above independent and dependent variable transformations in the KS, DS and other formulations [15]. These formulations exactly solve the two body portion and have automatic stepsize and energy control by including time and energy elements in the canonical formulation, as opposed to adding the time equation and control terms onto the Cowell formulation. The remaining problem with these formulations is that some of the dependent variables are slow and some are fast. Traditionally, "slow" means the variable is constant in unperturbed motion. The integration step must be smaller to account for the fast variables. Analytical [15] and numerical [7] averaging techniques are being formulated which smooth out these fast variations.

Two Scheifele [15] DS formulations are considered in this report.

In the first, we begin with the canonical equations of motion for the Cartesian phase space dependent variables with time as the independent variable. Phase space is extended by adding the energy-time conjugate dependent variables. This allows transformation to an independent variable which is linear in the true anomaly. Canonical transformations are made to the spherical phase space then to elements similar to Delaunay's. Of these dependent variables, seven are slow and one is fast (the true anomaly). The fast variable is very fast and the equations of motion have periodic terms multiplied by the fast variable for non-conservative forces (mixed secular terms). These stability and accuracy reducing problems are eliminated by further transforming the dependent and independent variables.

The DS independent variable is thus the true anomaly plus a constant and the dependent variables are:

$\alpha_1 = \phi$ = true anomaly	fast
$\alpha_2 = g$ = argument of pericenter	slow
$\alpha_3 = h$ = longitude of ascending node	slow
$\alpha_4 = \ell$ = time element	fast
$\alpha_5 = \Phi$	slow
$\alpha_6 = G$ = angular momentum	slow
$\alpha_7 = H$ = third component of angular momentum	slow
$\alpha_8 = L$ = - energy	slow

The angular momentum element (integral in Kepler's second law) is

used both as a dependent variable and in transforming the independent variable since from (2.2-1) $r^2 \frac{ds}{dt} = k$. The relations between the Cartesian extended phase space vector (2.1) and the DS elements are:

$$\phi = \text{sign (position} \cdot \text{velocity)} \arccos\left(\frac{p - r}{er}\right)$$

$$g = \arcsin\left(\frac{X_3}{r \sin i}\right) - \phi$$

$$h = \arctan\left(-\frac{G_1}{G_2}\right)$$

$$\ell = t - \frac{\mu}{(2L)^{3/2}}\left(E - \phi - \frac{re}{p}\sqrt{1 - e^2}\sin\phi\right)$$

$$\delta = G - \sqrt{G^2 + 2r^2V} + \frac{\mu}{2L}$$

$$G = \|\text{position x velocity}\|$$

$$H = G_3$$

$$L = X_8 = -\tfrac{1}{2}\,\text{velocity}^2 + \frac{\mu}{r} - V$$

where:

(G_1, G_2, G_3) = position x velocity

V = perturbing potential

μ = gravitational const. x $(M + m)$

$t = X_4$

$$\sin i = \text{sign}(H)\sqrt{1 - \frac{H^2}{G^2}}$$

$$p = \frac{1}{\mu}\left(G - \Phi + \frac{\mu}{2L}\right)^2$$

$$e = \sqrt{1 - \frac{2Lp}{\mu}}$$

$$r = p(1 - e\cos\phi)^{-1}$$

$$E = 2\arctan\left(\sqrt{\frac{1-e}{1+e}}\tan\tfrac{1}{2}\phi\right)$$

Details of transforming the differential equations to get $\frac{d\alpha}{ds}$ are given in [16]. This is integrated to get an α value which is transformed back to X.

Figures 4 and 5 graph these elements v.s. true anomaly for the first revolution for J_2 only, and Figures 6 and 7 for J_2 and the moon. Except for α_1 and α_4, they are periodic and the range of variation of α_4 is by far the greatest. Even though α_5 and α_6 are constant without perturbations, as soon as J_2 is added their variation is of the order of α_1. Any analysis based on their variation remaining small must be modified. α_2 and α_3 also vary but quite slowly. α_7 remains constant with J_2 and α_8 with all conservative perturbations, as expected.

When the moon is added, the variation of α_5, α_6, and α_7 is 10^2 to 10^3 greater than that of α_1 but it is still less than α_4. The remaining elements vary slowly. The greatest variation is near T = 4.4 which is at apogee (the point nearest the moon's orbit (Figure 3) <u>not</u> the point nearest the moon (Figure 1)).

Since the DS formulation was geared toward the central body being the main potential source, it is not surprising that the moon causes such gross "misbehavior" which can cause stability and truncation problems. This points to the necessity of using stepsize control when perturbations other than the central body are present.

In the second formulation considered, Scheifele has tried to slow the fast variables by analytically averaging the high frequency terms due to J_2 out of the equations by applying the von Zeipel algorithm. Ideally, this will allow larger stepsizes near the central body which will more than compensate for the increased computing necessary to make the extra transformation. Using the generating function S_1, a transformation is made from α to α', the "bblateness elements" OB. These"intermediate"elements are almost canonical since terms of order ϵ^2 have been ignored in the transformation.

If $\quad q = G - \frac{1}{2}\Phi + \dfrac{\mu}{2\sqrt{2L}} \quad$ and

$$(2.2\text{-}1)\quad S_1 = \left(-\frac{1}{2}\frac{eb}{pq} + \frac{1}{3}\frac{e}{pq}\right)\sin\phi + \frac{1}{2}\frac{eb}{pq}\sin(\phi + 2g) + \frac{1}{4}\frac{b}{pq}\sin(2\phi + 2g) + \frac{1}{12}\frac{eb}{pq}\sin(3\phi + 2g)$$

then the relation between α and α' is:

$$(2.2\text{-}2)\quad \alpha'(\alpha) = \alpha + \epsilon\left(\frac{\partial S_1}{\partial \alpha_5}, \ldots, \frac{\partial S_1}{\partial \alpha_8}, -\frac{\partial S_1}{\partial \alpha_1}, \ldots, -\frac{\partial S_1}{\partial \alpha_4}\right) = \alpha + \epsilon S(\alpha) \quad .$$

In transforming the differential equations, we first compute $\frac{d\bar{\alpha}}{ds}$ as for the DS elements.

From (2.2-2), we compute the Jacobian

$$\frac{\partial \bar{\alpha}'}{\partial \bar{\alpha}} = I + \epsilon \frac{\partial \bar{S}}{\partial \bar{\alpha}} \tag{2.2-3}$$

and form

$$\frac{d\bar{\alpha}'}{ds} = \frac{\partial \bar{\alpha}'}{\partial \bar{\alpha}} \frac{d\bar{\alpha}}{ds} = \frac{d\bar{\alpha}}{ds} + \epsilon \frac{\partial \bar{S}}{\partial \bar{\alpha}} \frac{d\bar{\alpha}}{ds} \quad .$$

The dynamic and numerical stability of the OB elements thus depends on that of the DS elements and on the second partials of the generating function S_1. Integrating $\frac{d\bar{\alpha}'}{ds}$ yields a value of $\bar{\alpha}'$. To find $\bar{\alpha}$ from $\bar{\alpha}'$, we have $\bar{\alpha}(\bar{\alpha}') = \bar{\alpha}' - \epsilon S(\bar{\alpha})$ which is a nonlinear transformation and must be iterated, thus increasing the computing time. This transform recovers the J_2 high frequency terms. The transform from $\bar{\alpha}$ to X recovers the two body portion and yields the Cartesian state. These back transforms must be done at each step in order to evaluate the forces (Section 3.2).

3.0 EQUATION INTEGRATION

3.1 Integrators

The orbits are generated with two basic types of integrators. The first is the seventh order Runga-Kutta method RK7(8) of Fehlberg [6]. This is the highest order R-K method in use today. An estimate to the

local truncation error is obtained by evaluating its leading term. Thirteen function evaluations per step are required. Following these evaluations the local truncation error estimate is compared to a user supplied tolerance, TOL. If the estimate exceeds TOL, a smaller stepsize is chosen and 12 of the evaluations are repeated with this new stepsize. The stepsize is reduced until the estimate is less than TOL. Then this value for the solution is accepted at this step and we proceed to the next step with a specified stepsize. An option is available to override the stepsize control and integrate with a fixed stepsize.

The second integrator used is the Adams, nonsummed, ordinate form [8]. In this study, we used fixed stepsizes; the smallest being 10^{-3} of the largest which is a greater range than comparable studies. This was done to get a complete idea of the range of stability and accuracy that is possible with the DS elements. The orders used range from 2 to 15. Order 15 is three or four orders higher than commonly used in orbit generation. The fixed correcting algorithms used are PE, PEC, PECE, and $PE(CE)^2$ which require one to three function evaluations per step. The coefficients were computed in 25D, using a CDC 3350.

The program will accept cyclic integrators [5], [18], [21] and a thorough study using these should be done. The optimized ones [14] are especially more stable and accurate than the traditional multistep integrators and relatively improve with high eccentricities. With stepsize control they will probably require fewer stepsize changes.

3.2 Program Description

Two programs are used. The first is for the DS elements.

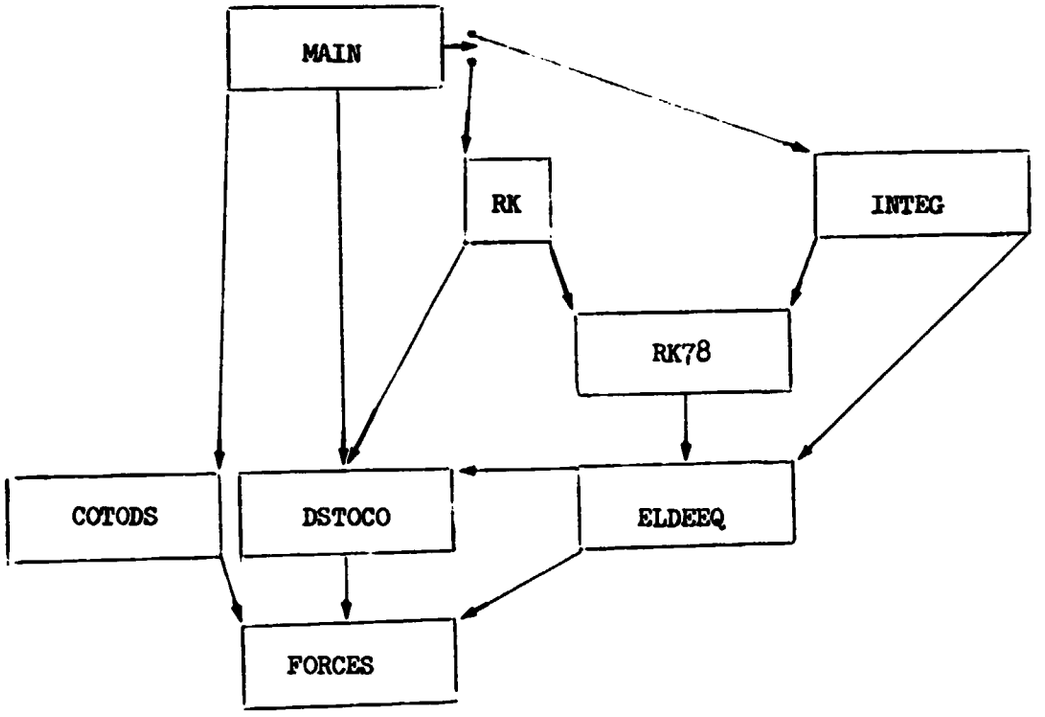

MAIN: Initializes Cartesian vector, transforms to initial DS vector, calls either RK or INTEG, then transforms final DS to Cartesian coordinates.

DSTOCO, COTODS: Transformations between DS and Cartesian vectors (Section 2.2).

FORCES: Computes potentials and forces in Cartesian coordinates.

ELDEEQ: Converts potentials and forces from Cartesian coordinates to be used in the DS differential equations for $\frac{d\alpha}{ds}$.

RK78: Runga-Kutta integration from one step to the next (Section 3.1).

INTEG: Uses RK78 to compute starting values for traditional or cyclic multistep, predictor-corrector integration (Section 3.1) stepping along in true anomaly (T) until X_4 > final time (t_f). Now consider X_4 to be a function of true anomaly X_4 (T). We wish to find that T value, T_f, where $X_4(T_f) - t_f = 0$. Using Newton's method:

$$T_{i+1} - T_i = - \frac{X_4(T_i) - t_f}{\frac{d}{dT}(X_4(T_i) - t_f)} \tag{3.2-1}$$

where the denominator is approximated by $\frac{X_4(T_i) - X_4(T_{i-1})}{T_i - T_{i-1}}$.

T_{i+1} then converges to T_f. Iteration is stopped when $T_{i+1} - T_i \leq$ DTTOL which is specified on input. Evaluating the DS vector at $T_{i+1} \approx T_f$ will yield $X_4 \approx t_f$ and this final solution will automatically include any timing error (Section 2.2).

RK: Controls RK78 as it steps along in true anomaly (Section 3.1) until $X_4 > t_f$ then proceeds as in INTEG.

The second program is for the OB elements.

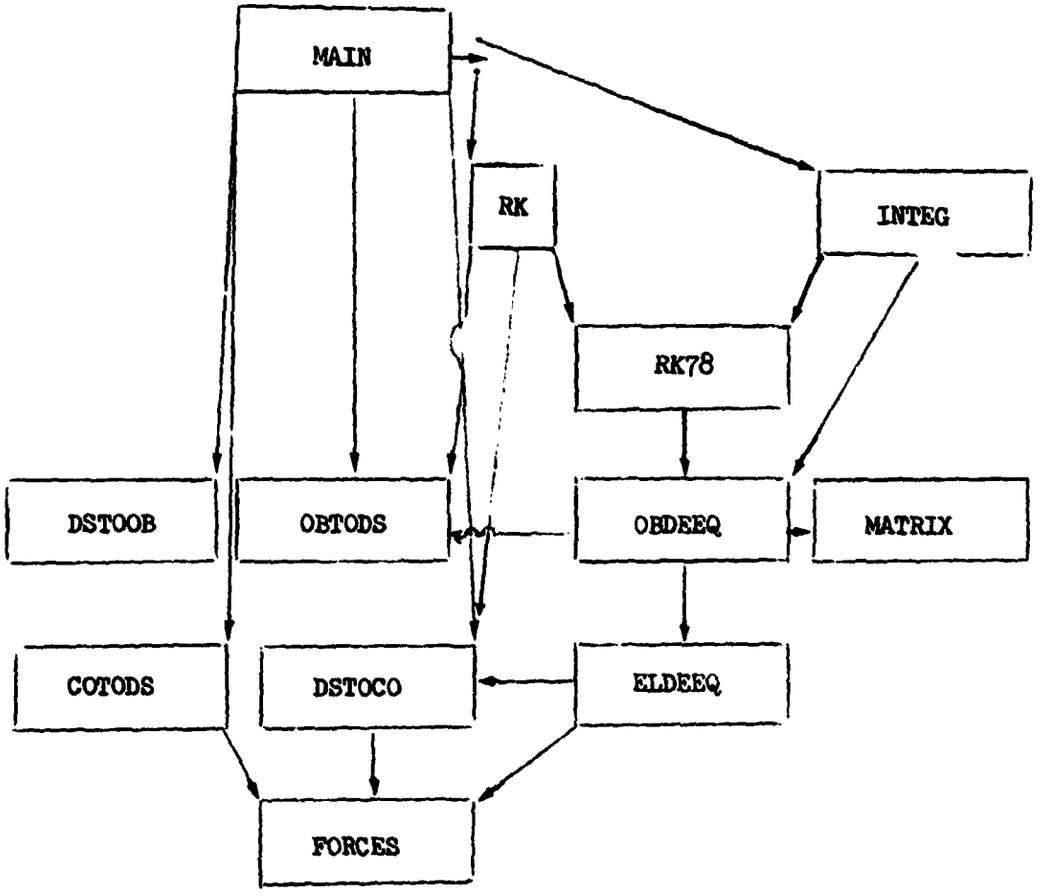

MAIN: Initializes Cartesian vector, transforms to initial DS and OB vectors, calls either RK or INTEG, then transforms final OB to DS to Cartesian coordinates.

DSTOOB, OBTODS: Transformations between DS and OB vectors (Section 2.2).

MATRIX: Computes the Jacobian $\frac{d\bar{\alpha}'}{d\bar{\alpha}}$ (Section 2.2).

OBDEEQ: Computes $\frac{d\alpha'}{ds}$ from $\frac{\partial\bar{\alpha}'}{\partial\bar{\alpha}}\ \frac{d\alpha}{ds}$.

INTEG and RK now integrate the OB vector. At this writing, several bugs are being worked out of the OB version of the program, so we have no numerical results yet to report. A preliminary version of this program with the Runga-Kutta integrator is due to G. Scheifele [15].

4.0 EFFICIENCY

The reference solutions were generated by converting the program to a CDC 3350 with 25D and running it with the R-K variable step with TOL = DTTOL = 10^{-18} (Section 3). Having both Cartesian and DS solutions allows an analysis of the effects of the transformations. We are confident the reference solutions are accurate to 16D. Figures 2 through 7 graph the solution.

Comparison runs for the DS elements were made on a Xerox Sigma 7 which has the same word structure as the IBM 360 (16D), allowing comparisons with runs on that machine. A total of 48 curves were generated (Figures 8 through 15 and Table 1) each with approximately 6 stepsizes, ranging over a factor of 10^3, for a total of 288 successful runs.

TABLE 1

SUMMARY OF EFFICIENCY CURVES FOR THE DS FORMULATION

Fig. No.	Perturbations	Integrator	Algorithm	Orders
8	J_2 only	RK	fixed step variable step	7
	J_2 and moon	RK	fixed step variable step	7
9	J_2 only	Adams	PE	6, 15
	J_2 and moon	Adams	PE	6, 15
10	J_2 only	Adams	PEC	2 - 15
11	J_2 only	Adams	PECE	2 - 15
12	J_2 only	Adams	$PE(CE)^2$	2 - 15
13	J_2 and moon	Adams	PEC	2 - 15
14	J_2 and moon	Adams	PECE	2 - 15
15	J_2 and moon	Adams	$PE(CE)^2$	2 - 15
16	J_2 only	Adams	all	envelope
17	J_2 and moon	Adams	all	envelope

The first vertical scale is the Euclidean norm of the Cartesian position error in meters. This includes the implicit error due to the timing error. The second scale is the relative error which is the error divided by the final r value. A relative error of 10^{-4}, for example, means there are four significant digits of accuracy in the satellites position.

The first horizontal scale is the "effective stepsize", h, in radians. h is normalized to be the actual stepsize for the standard PECE (2 function evaluations per step) and is adjusted for other correcting algorithms according to the number of function evaluations. This enables a direct comparison of computing times for different algorithms. The formula is:

$$h = \frac{2(\text{arc length})}{(\text{total \# fctn. evaluations})} \tag{4.0-1}$$

which is twice the average distance between evaluations. The second and third scales are the total number of evaluations and the Sigma 7 CPU seconds not including factors for the amount of core used or swaps. This will allow comparisons with other machines.

Let p = the order of the integrator and d depend on the integrator and on the high derivatives of the differential equations thus on the formulation used. In the log-log graphs in the truncation limited region, ideally:

$$\log(\text{error}) \lesssim p \log h + \log d \quad . \tag{4.0-2}$$

The curves should be straight lines with slope = order. A good combination of formulation and integrator will yield a smaller d, thus yielding an overall efficiency improvement. This is one reason for optimizing integrators [14, 18, 19] in addition to improving stability, and for considering the combined effects of formulation and integrator [12, 17].

4.1 Runga - Kutta

In Figure 8, the points for $h \gtrsim .2$ should be ignored since most of the function evaluations are involved in the finishing procedure (Section 3.2) and do not accurately represent efficiency. Otherwise, the curves are generally linear with both fixed step slopes $\gtrsim 10$ which is three orders higher than expected. The variable step curves are even steeper, so much so that the choice of TOL is very critical to the propogated error.

The moon's perturbation increases the error by a factor of 10^7 to 10^8, possibly caused by a larger value of d (4.0-2). This accuracy degradation is not as great with Adams integrators. The computing time is simultaneously increased due to the additional computations. Notice the two CPU scales.

4.2 Adams, Conservative Perturbation

Figures 9 - 12 show quite a regular behavior and all modes remain stable. Figure 12, $PE(CE)^2$, curves exhibit what might be termed ideal behavior. What we will call a "pivot point" occurs at (h, error) $\approx$ (.3, 10^3 m) where all curves cross almost simultaneously. At smaller h, higher orders are more efficient; at larger, they are less efficient. The lines should cross due to the expected different slopes (4.0-2) but this does not explain why they all cross at nearly the same point.

At the largest h run, we are taking only about seven steps for a whole revolution. The stability is remarkable. At even larger h, the

higher orders will become unstable first.

As h decreases, the error reaches a minimum then increases as roundoff takes over causing a "dip" near (h, error) = (.5, 13.5 significant digits) which is almost all we can expect from this 16D machine. The orders 2 and 4 truncation errors are still too large for the total error to be seriously effected by roundoff. At even smaller h, these should also show a dip.

Figures 9, 10, 11 resemble one another. They have what look like truncation limited regions with the pivot point and dip region moving to the left in h as the corrector influence increases in a definite trend.

algorithm	PE	PEC	PECE	$PE(CE)^2$
pivot h		1.6	.6	.3
dip h	.6	.2	.1	$\lesssim$ .06

However, these dips occur at less than 9D, implying their cause is not roundoff.

As h decreases, all orders become parallel with slope = 1 for PE and slope = 2 for PEC and PECE (Table 2). This is not a truncation limited region since the slopes are equal and not a roundoff limited region since errors decrease with h. We hypothesize the explanation for these phenomena lies in the truncation error coupling of the formulation to the integrator.

4.3 Adams, Non-Conservative Perturbation

Figures 9, 13, 14, 15 with the lunar perturbation are not as regular as with J_2 only and the higher orders do become unstable. In Figure 15, the $PE(CE)^2$ curves are nearly straight lines at small to medium h with higher order methods being steeper as expected in a truncation region (4.0-2); however, the near equality of the slopes was not expected. At the smallest h run, truncation is still too large for roundoff to give a dip.

There is a pivot near h = .05; however, to the right there are convex and concave curves, so the picture is not as clear as with J_2 only.

Orders 10, 12, and 15 became unstable and the higher orders have smaller stability regions. It is surprising the order 8 remained stable at h giving only 7 steps per revolution.

Figures 9, 13, 14 resemble one another. Orders 12 and 15 always become unstable after having a dip at error values too large to be caused by roundoff. The point of instability (and the dip) moves to the left with increasing corrections (as with J_2 only), so the stability region becomes smaller with increasing corrections.

There appear to be no trunction nor roundoff regions at all. The curves just twist around each other in a tight bundle with any order 4 - 8 being as efficient as another (2 is also close), except the 12 and 15 are more efficient at the dip and less when they are unstable. The bundle has slope approximately 1.6 for PE and 2.3 for PEC and PECE which is analogous to the small h result for J_2 only (Table 2).

TABLE 2

SLOPES OF EFFICIENCY CURVES

Algorithm	Stepsize Range	Orders of Adams Methods 2	4	6	8	10	12	15
				J_2 Only				
PE	small	-	-	1.0	-	-	-	1.0
	medium	-	-	*	-	-	-	*
	large	-	-	3.9	-	-	-	15.0
PEC	small	2.0	2.0	2.0	2.0	-	2.0	1.9
	medium	2.0	2.0	2.0	*	-	*	*
	large	2.7	4.3	5.0	6.6	-	8.0	12.0
PECE	small	2.0	2.0	2.0	2.0	2.0	2.0	2.0
	medium	1.8	*	*	*	*	*	*
	large	2.8	4.0	4.8	6.0	7.5	8.0	17.0
$PE(CE)^2$	small	2.0	4.0	*	-1.0	-1.0	-1.0	-1.0
	medium	1.7	4.0	6.3	*	*	*	*
	large	2.8	4.1	5.0	6.6	8.6	8.0	12.0
				J_2 and Moon				
PE	all	-	-	1.6	-	-	-	*
PEC	small	2.0	2.6	2.6	2.6	-	2.7	2.5
	medium	1.8	2.2	*	1.7	-	*	*
	large	2.4	2.3	*	2.7	-	∞	∞
PECE	small	1.9	2.6	2.8	1.8	-	2.7	2.5
	medium	1.9	2.5	2.6	2.2	-	6.4	*
	large	2.3	2.4	1.8	1.9	-	∞	∞
$PE(CE)^2$	small	1.9	3.9	6.0	6.7	-	7.5	7.5
	medium	2.3	4.2	5.0	5.2	-	6.7	∞
	large	2.5	2.1	2.4	2.0	-	∞	∞

* Large curvature in this region
- No runs

4.4 Efficiency Envelopes, Comparisons

In the R - K curves (Figure 8), we see that with J_2 only the fixed step algorithm is more efficient. This is probably because the step-size control is not optimal. With the moon variable step is more efficient for errors $\lesssim$ 10 meters, but less efficient for larger acceptable errors. These results and Figures 2 and 3 show that stepsize control is not needed for J_2 only, but the stepsize at apogee is 1/10 that at perigee with the moon indicating that stepsize control is necessary in this case.

Aligning the vertical and horizontal scales of the J_2 only curves allows comparison of the most efficient orders for each algorithm in Figure 16. There is one curve for each algorithm. The PEC graph was shifted slightly to the left of the PE graph due to the slightly greater CPU time. Algorithms with more corrections are generally steeper and there is an algorithm pivot point near (h, error) = (0.18, 1 m). These phenomenon resemble those of the different orders of a single algorithm; more corrections and higher order both lead to steeper curves (Table 2). The stability intervals are very large; not exceeded by our largest h.

Using orders greater than 12 generally does not significantly improve efficiency. Orders 12 and 15 dominate Figure 16.

The most efficient integration mode for errors < 1 m and h < .18 is $PE(CE)^2$ order 12 or 15. The most efficient for larger errors is PEC order 12 or 15. The maximum achievable accuracy is 13.5 D on the 16 D machine.

The most efficient orders for each algorithm with the lunar perturbation are sketched in Figure 17. More corrections and higher order lead to steeper curves and there is a pivot near (h, error) = (0.03, 100 m), but these phenomenon are not as clear as with J_2 only. More perturbations tend to confuse the picture. The stability intervals are still large, expecially for orders ≤ 8. Orders 6, 12, and 15 dominate this figure.

Since orders 12 and 15 become unstable and in their stability regions they are not much of an improvement over lower orders, it seems safer to use lower orders. The most efficient and reliable integration mode for errors $\lesssim$ 100 m and h $\lesssim$ .03 is PE$(CE)^2$ order 8. For larger errors it is PEC order 6. These are the same two algorithms as without the moon, but stability has forced us to lower orders.

Since the stability region for Adams PEC is ideally smaller than PECE and even PE [17 Table 1], it is surprising that with the DS formulation PEC is best at large stepsizes.

Comparing Figures 8, 16, 17, we see with J_2 only RK fixed step is as efficient as Adams PE$(CE)^2$ order 15 for errors < 1 m, but for larger allowable errors Adams PEC order 12 is most efficient. For J_2 only, the Adams integrator is more efficient at all stepsizes.

With J_2 and lunar perturbations RK variable step is most efficient for errors $\lesssim$ 100 m, but for larger errors Adams PEC is better.

REFERENCES

1. Beaudet, P. R., "The Testing and Comparison of Various Methods of Special Perturbations," CSC, 3000-08600-01 TM, January 1974.

2. Beaudet, P. R. and T. Feagin, "The Use of Back Corrections in Multistep Methods of Numerical Integration," Submitted SIAM J Numer. Anal., 1974.

3. Baumgarte, J., "Dynamic Stabilization of Perturbed Keplerian Motions," Celest. Mech., Vol. 5, 1972, 490.

4. Dallas, S. S. and E. A. Rinderle, "A Comparison of Cowell's Method and a Variation of Parameters Method for the Computation of Precision Satellite Orbits," JPL, TM 392-101, September 1972.

5. Donelson III, J. and E. Hansen, "Cyclic Composite Multistep Predictor-Corrector Methods, SIAM J. Numer. Anal., Vol. 8, 1971, 137-157.

6. Fehlberg, E. "Classical Fifth, Sixth, Seventh, and Eight Order Runga-Kutta Formulas with Stepsize Control," NASA, TR-R-287, October 1968.

7. Fuchs, A. J., "Averaging Technique Applications in Orbit Determination," Fifth Astrodyn. and Geodyn. Conf., NASA - GSFC, October 1973.

8. Henrici, P., "Discrete Variable Methods in Ordinary Differential Equations," Wiley, New York, 1968.

9. Janin, G., "Accurate Computation of Highly Eccentric Satellite Orbits," ESRO-ESOC, Germany, 1973.

10. Krogh, F. T., "Algorithms for Changing the Step Size," SIAM J. Numer. Anal., Vol. 10, No. 5,October 1973, 949-965.

11. Moore, W. H. and P. R. Beaudet, "The Testing of Fixed-Step Numerical Integration Processes for the Cowell Method of Special Perturbations," CSC, 9101-16200-01 TR, March 1973.

12. Narcozy, P. E., "The Reduction of Local Truncation Errors by Time Transformations," ASS Div. Dyn. Ast. - SIAM Conf., 1972.

13. Peñas, A., "Accurate Integration of Orbits Using Delaunay - Similiar Elements," NASA - GSFC, X-582-73-375, December 1973.

14. Pierce, S., "Analysis and Optimization of Cyclic Methods for Application in Orbit Computations," NASA Contractor Report CR-132826, Government Accession No. N 74-13292, July 1973.

15. Scheifele, G. and E. L. Stiefel, "Canonical Satellite Theory," ESRO-ESOC, 219/70/AR, February 1972.

16. Stiefel, E. L. and G. Schiefele, "Linear and Regular Celestial Mechanics," Springer-Verlag, New York, 1971.

17. Velez, C. E., "Notions of Analytic v.s. Numerical Stability as Applied to the Numerical Calculation of Orbits," AIAA Conf.

18. Chesler, L. G. and S. Pierce, "Applications of Generalized, Cyclic and Modified Numerical Integration Algorithms to Problems of Satellite Orbit Computation," System Development Corp., Santa Monica, TM-4717/000/00, March 1971.

19. Dyer, J., S. Pierce, D. Haney, and L. Chesler, "Generalized Multistep Methods in Orbit Computation: Studies in Existance Theory, Efficiency, Optimization," System Development Corp., Santa Monica, TM-4888/000/00, February 1972.

20. Long, A. C., K. S. Nimitz, and P. J. Cefola, "The Next Generation of Orbit Prediction Formulations for Artificial Satellites II," CSC, 9101-14600-01TR, November 1973.

21. Pierce, S. and L. Chesler, "Cyclic Correctors for Solving Class I and II Ordinary Differential Equations," SIAM Rev. Vol. 14, No. 1, January 1972.

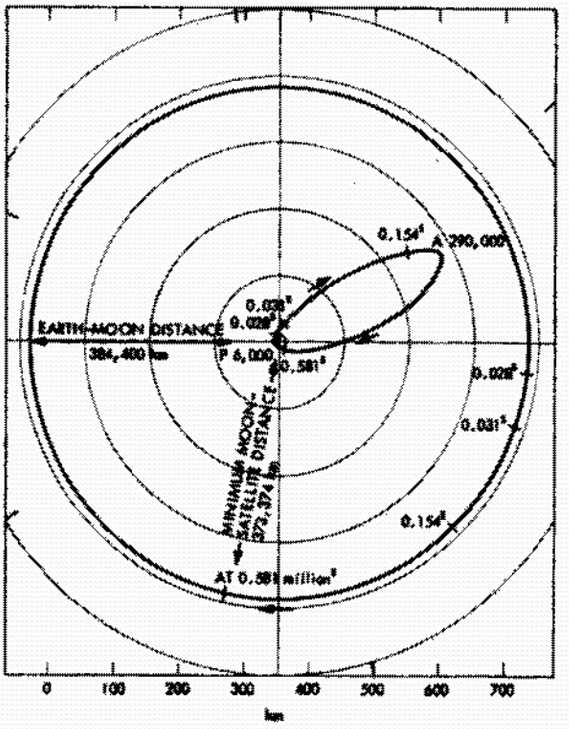

Fig. 1. Earth-Moon-satellite geometry: roughly sketched in the same plane; during first orbit; time marks on Moon and satellite orbits are 10^6s; distance in km; perigee and apogee marked P and A, respectively

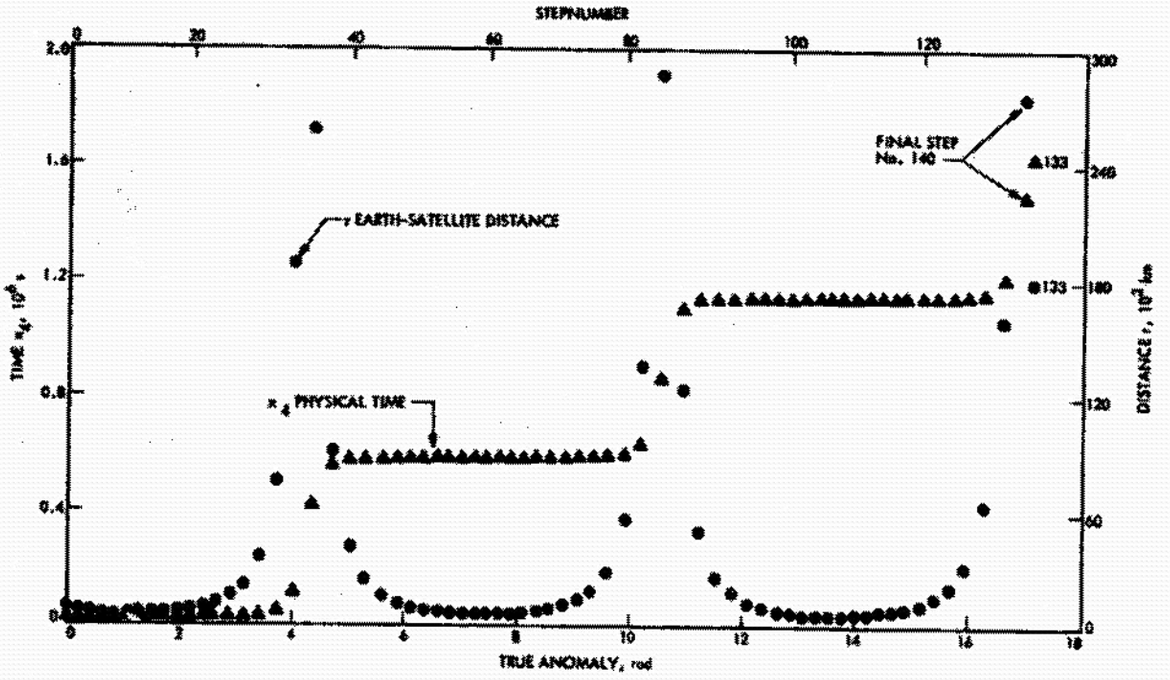

Fig. 2. Reference solution: Earth-satellite distance and physical time /s "true" anomaly and stepnumber; without moon; every second step is plotted

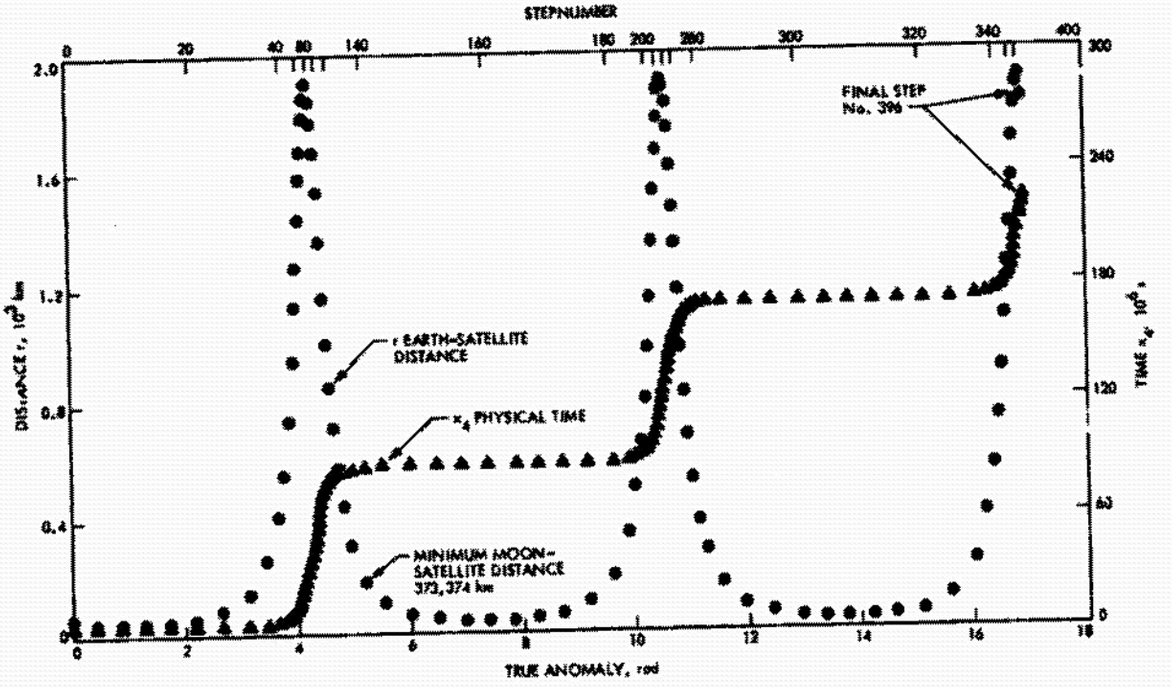

Fig. 3. Reference solution: Earth-satellite distance and physical time vs "true" anomaly and stepnumber; with moon; every fourth step is plotted

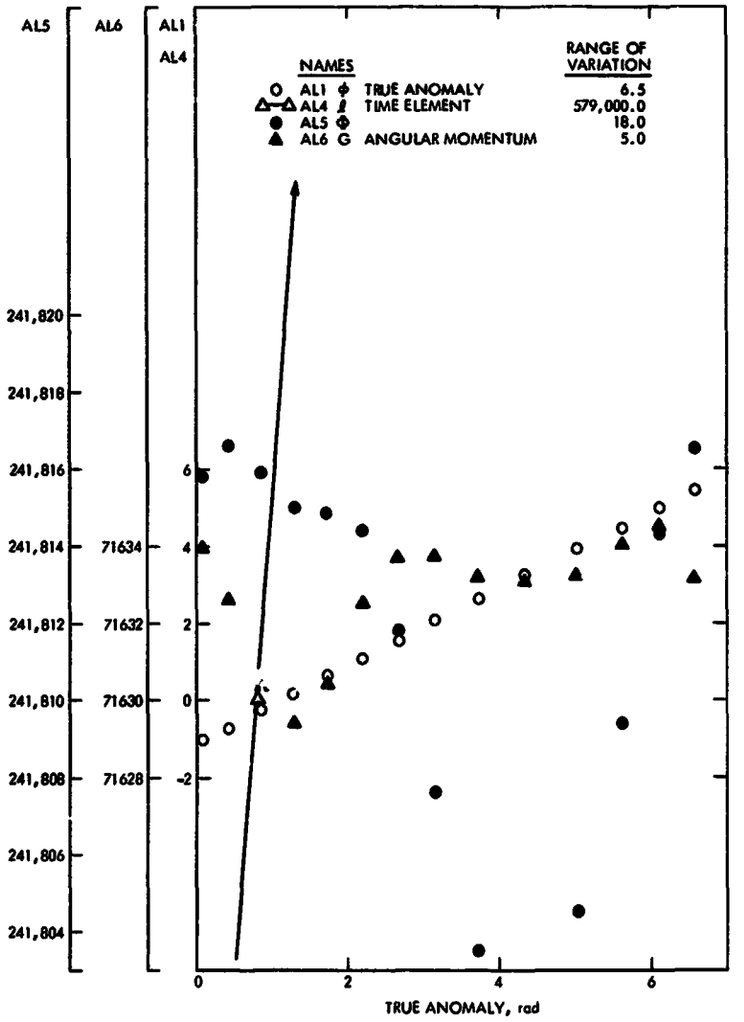

Fig. 4. Reference solution J2 only: for first orbit; quickly varying components of the DS elements; scale: 1 cm = 1 unit; compare to Fig. 2

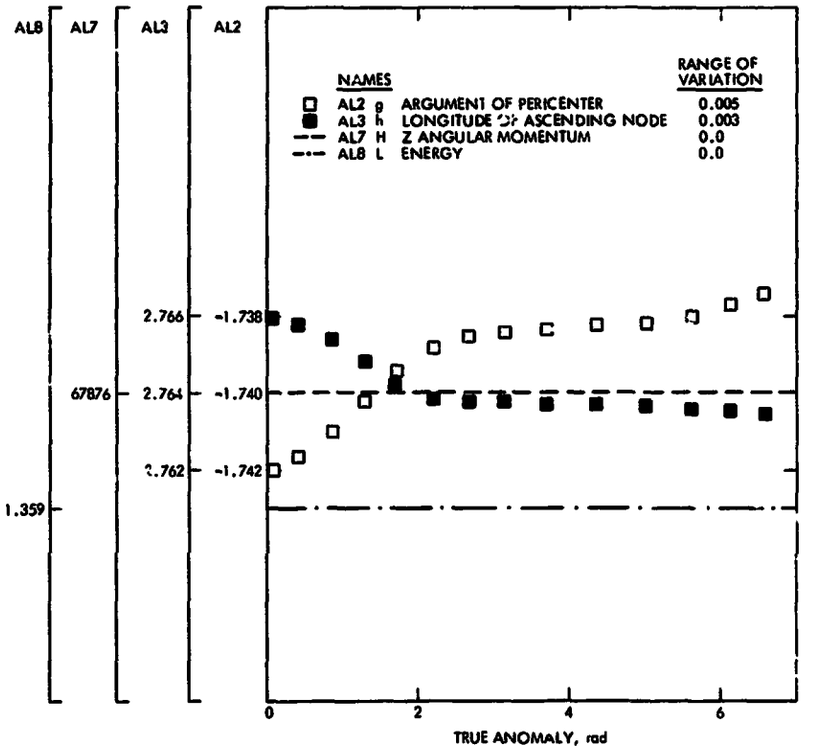

Fig. 5. Reference solution J2 only: for first orbit; slowly varying components of the DS elements; scale: 1 cm = 0.001 units; compare to Fig. 2

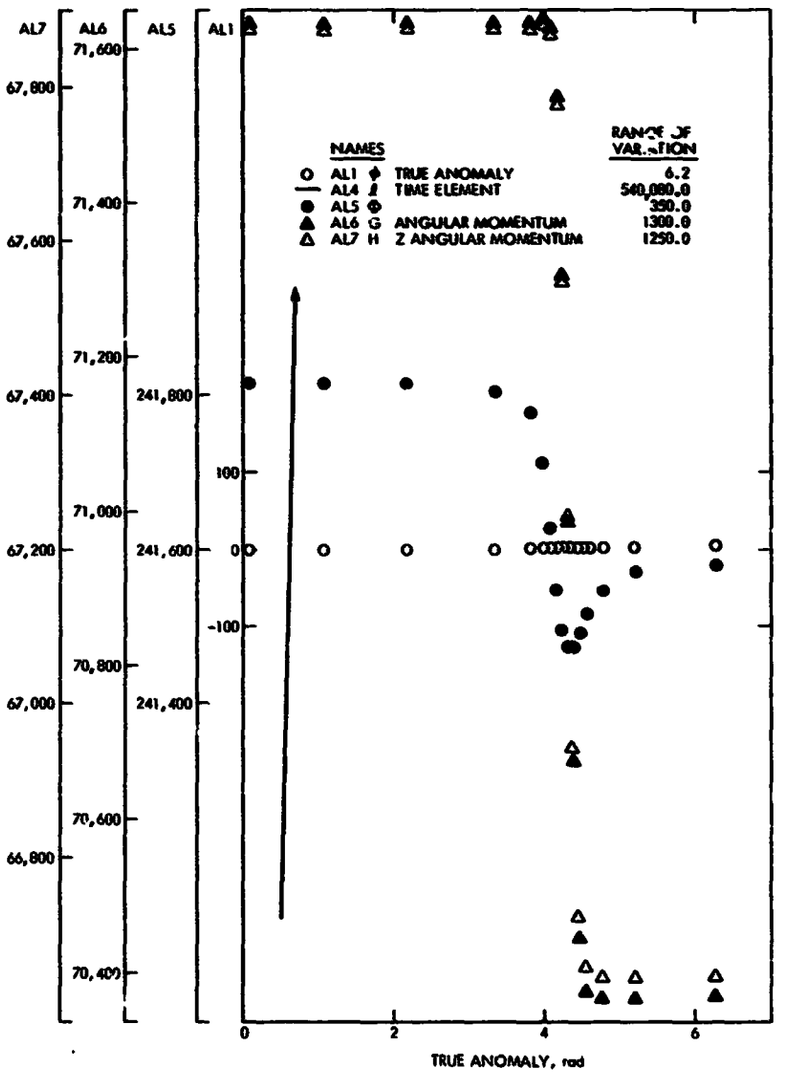

Fig. 6. Reference solution J2 and moon: for first orbit; quickly varying components of the DS elements; scale 1 cm = 50 units; compare to Fig. 3

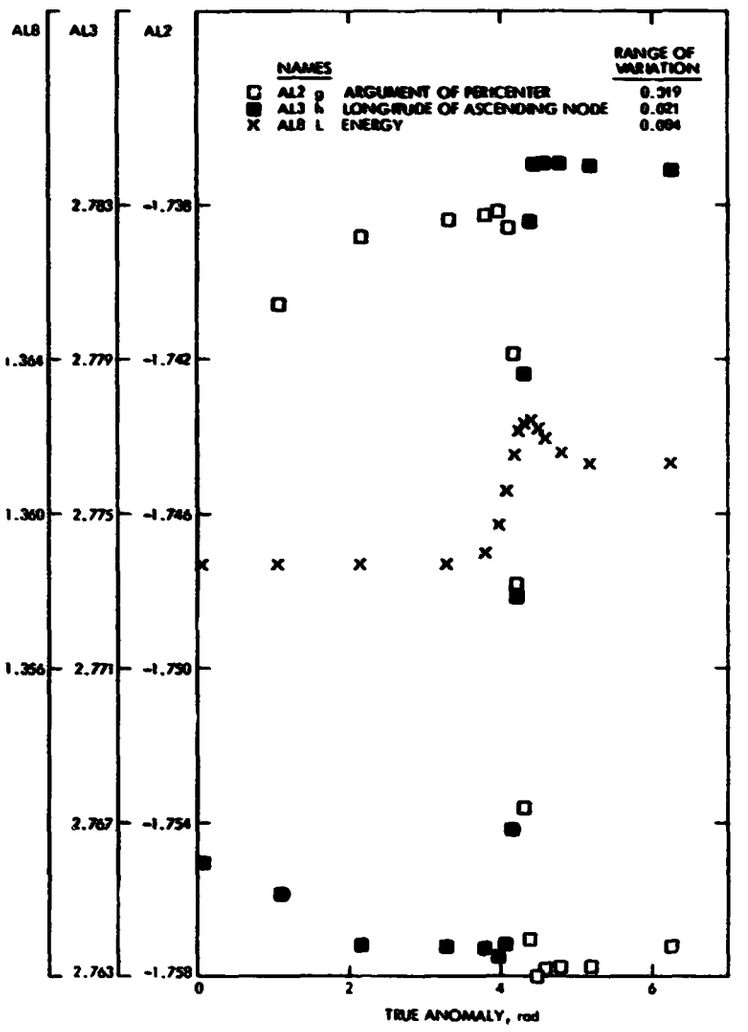

Fig. 7. Reference solution J2 and moon: for first orbit; slowly varying components of the DS elements; scale: 1 cm = 0.001 units; compare to Fig. 3

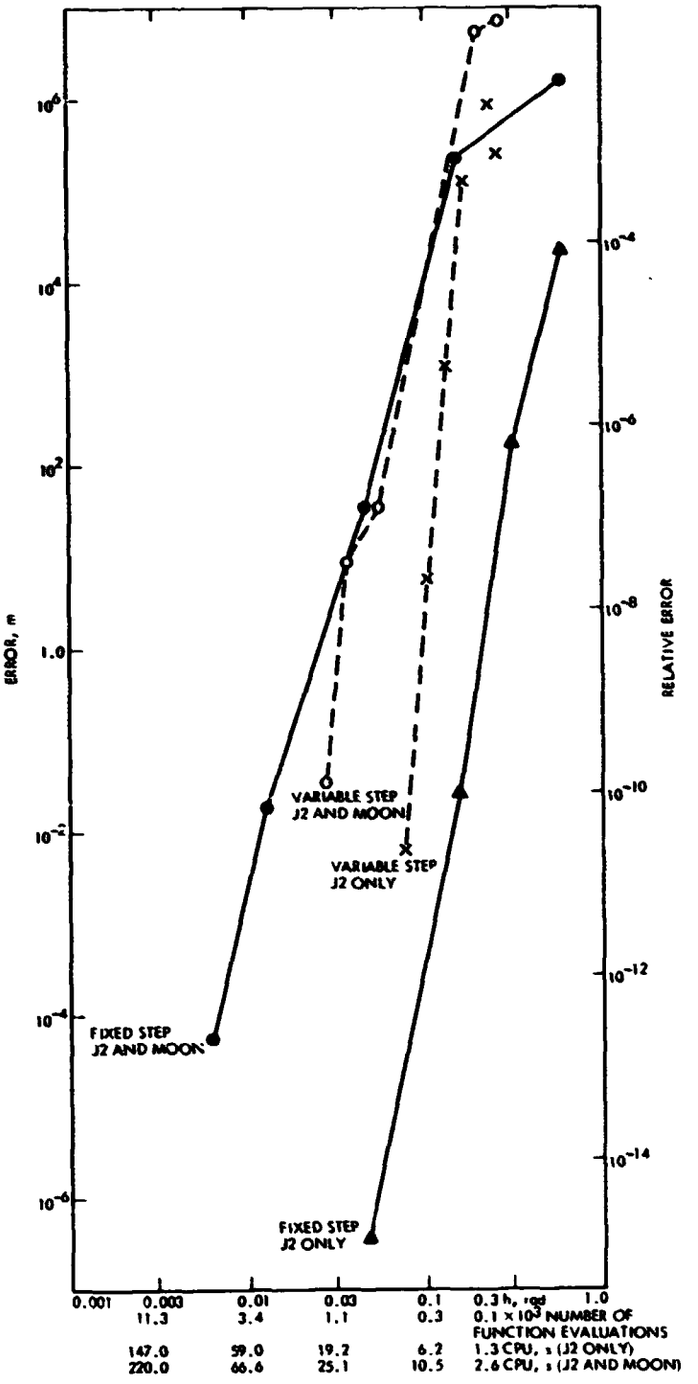

Fig. 8. Efficiency curves Runga-Kutta

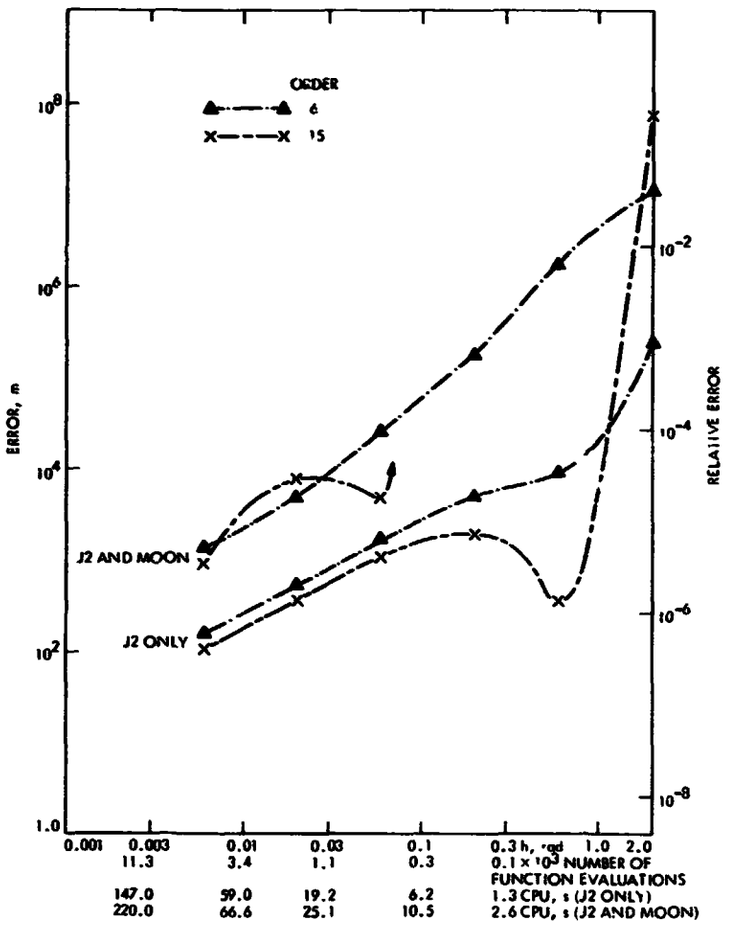

Fig. 9. Efficiency curves Adams PE

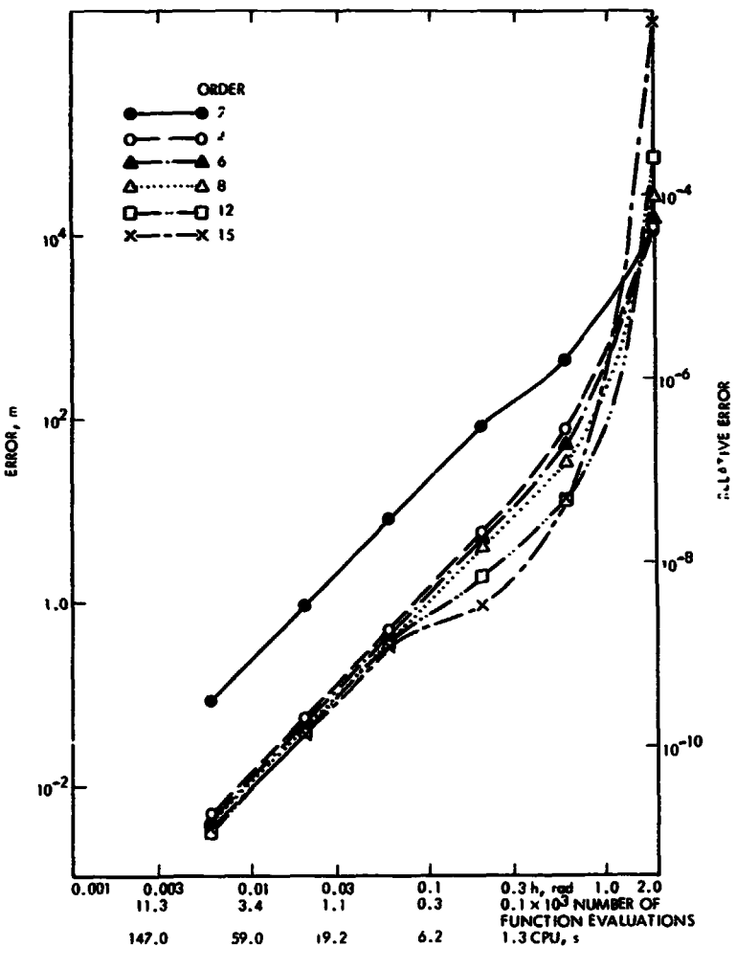

Fig. 10. Efficiency curves J2 only Adams PEC

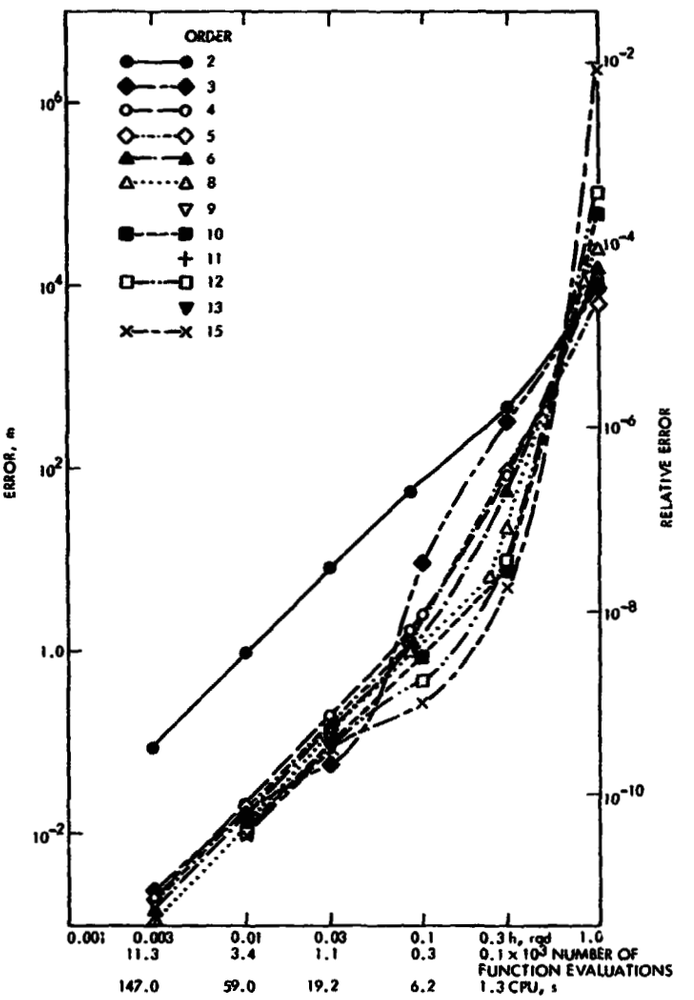

Fig. 11. Efficiency curves J2 only Adams PECE

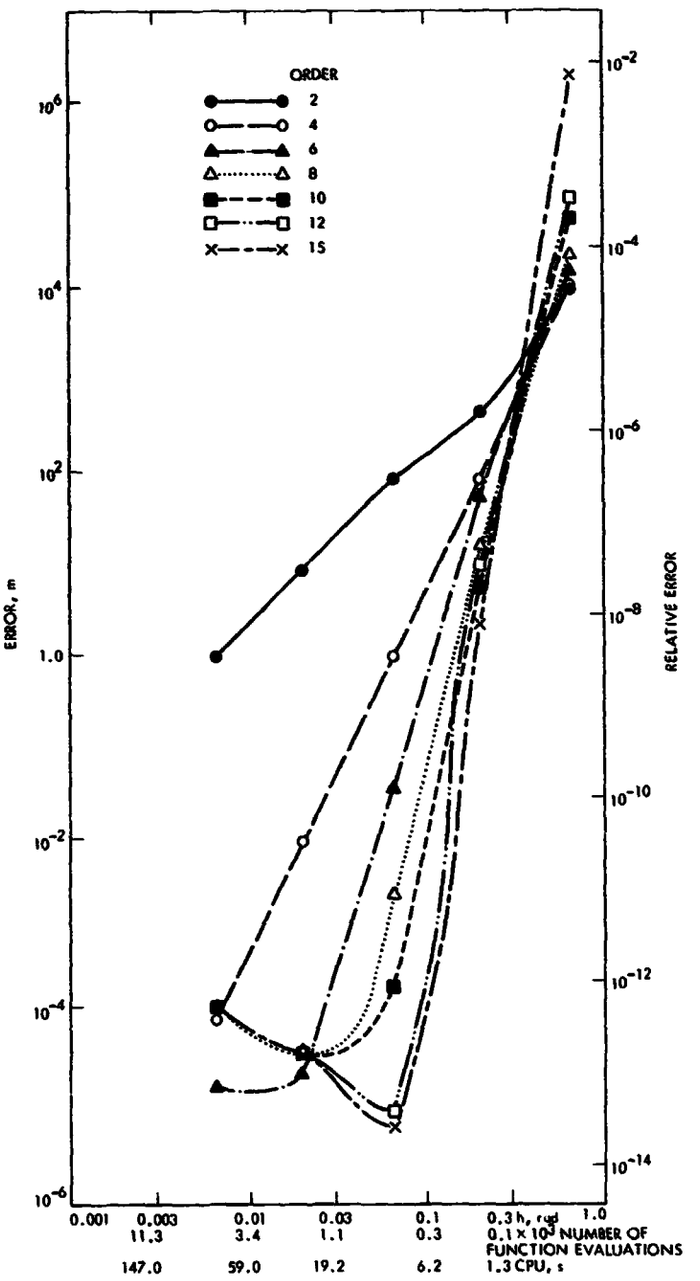

Fig. 12. Efficiency curves J2 only Adams PE(CE)^2

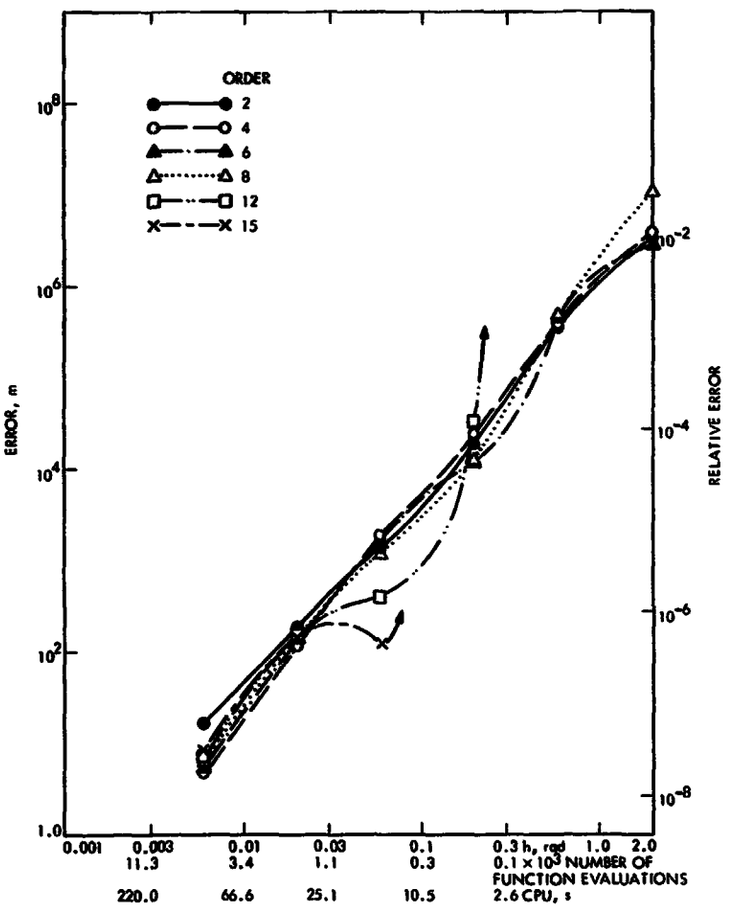

Fig. 13. Efficiency curves J2 and moon Adams PEC

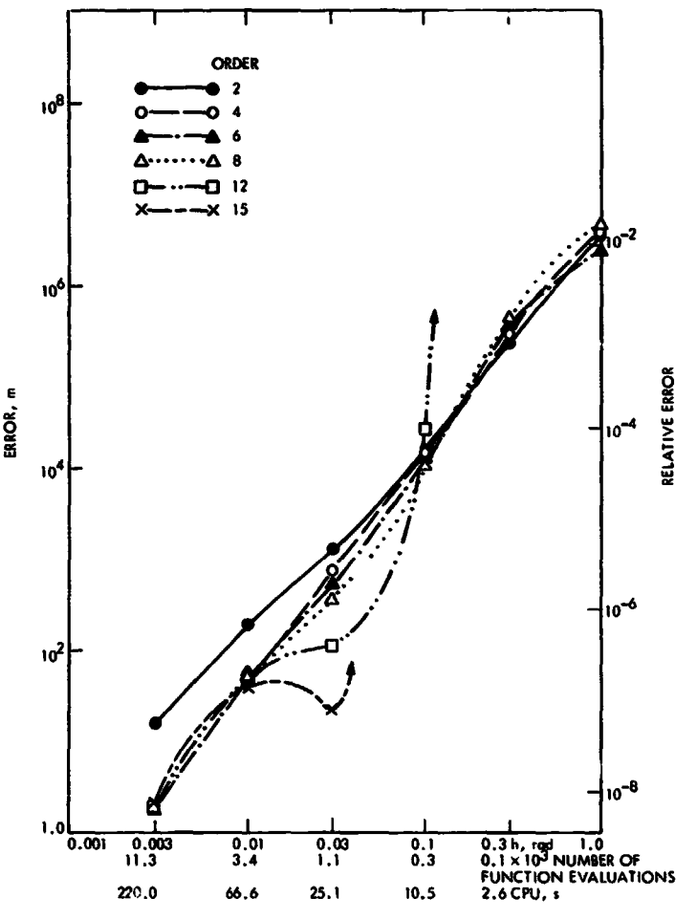

Fig. 14. Efficiency curves J2 and moon Adams PECE

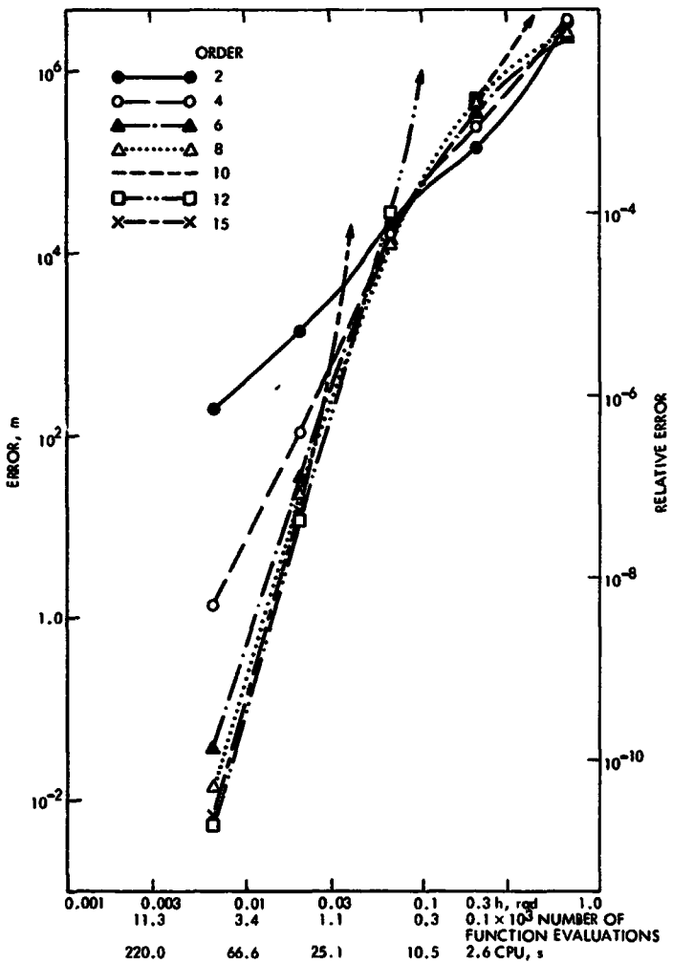

Fig. 15. Efficiency curves J2 and moon Adams PE(CE)^2

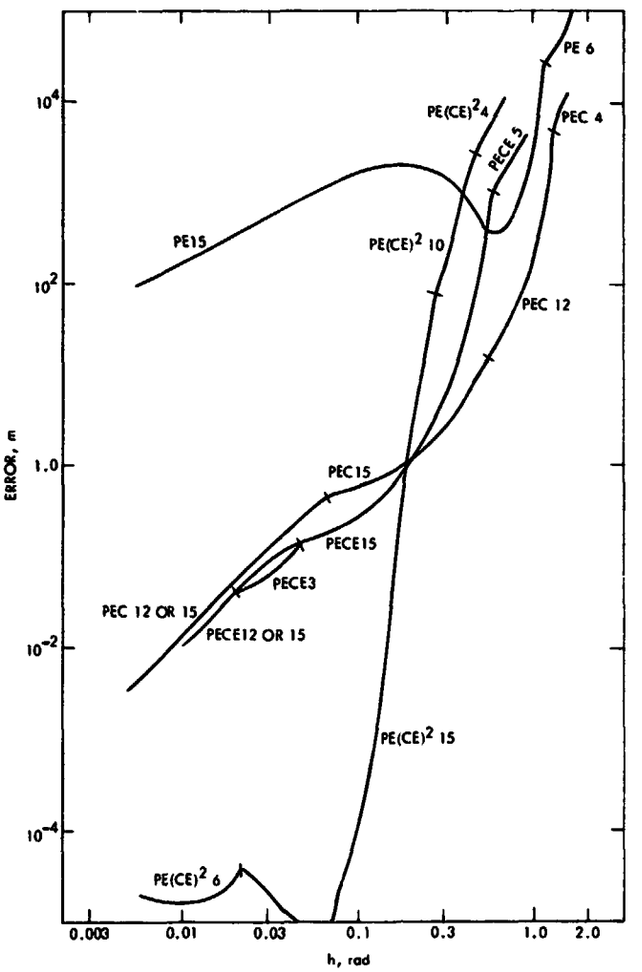

Fig. 16. Efficiency envelopes J2 only Adams

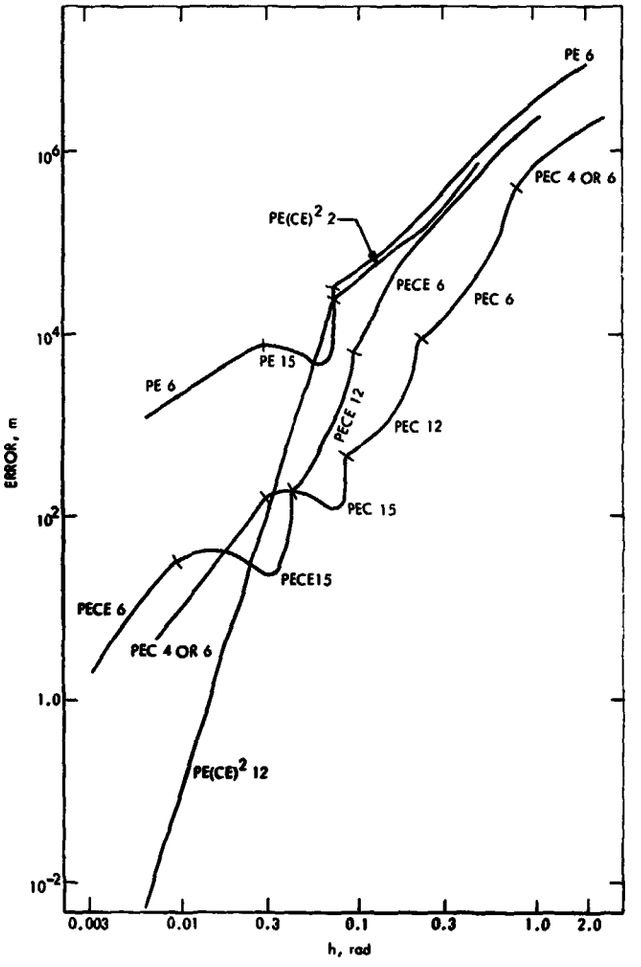

Fig. 17. Efficiency envelopes J2 and moon Adams

NASA — JPL — Coml., L.A., Calif.